

POLAFORMER: POLARITY-AWARE LINEAR ATTENTION FOR VISION TRANSFORMERS

Anonymous authors

Paper under double-blind review

ABSTRACT

Linear attention has emerged as a promising alternative to softmax-based attention, leveraging kernelized feature maps to reduce complexity from quadratic to linear in sequence length. However, the non-negative constraint on feature maps and the relaxed exponential function used in approximation lead to significant information loss compared to the original query-key dot products, resulting in less discriminative attention maps with higher entropy. To address the missing interactions driven by negative values in query-key pairs, we propose a polarity-aware linear attention mechanism that explicitly models both same-signed and opposite-signed query-key interactions, ensuring comprehensive coverage of relational information. Furthermore, to restore the spiky properties of attention maps, we provide a theoretical analysis proving the existence of a class of element-wise functions (with positive first and second derivatives) that can reduce entropy in the attention distribution. For simplicity, and recognizing the distinct contributions of each dimension, we employ a learnable power function for rescaling, allowing strong and weak attention signals to be effectively separated. Extensive experiments demonstrate that the proposed PolaFormer improves performance on various vision tasks, enhancing both expressiveness and efficiency by up to 4.6%.

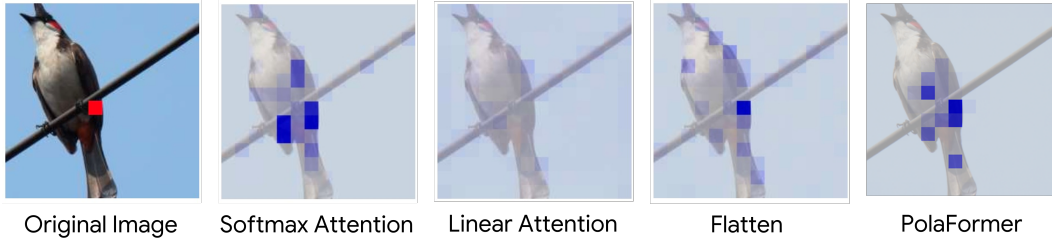


Figure 1: **Attention weight visualization.** Unlike prior linear attention approaches ((Katharopoulos et al., 2020) the 3rd and (Han et al., 2023a) 4th plots) that generate uniform responses, the proposed PolaFormer captures a more accurate query-key interaction with lower entropy, closely resembling softmax while maintaining linear complexity.

1 INTRODUCTION

Transformers have demonstrated remarkable success across a broad range of vision tasks (Yuan et al., 2021b; Cai et al., 2022). The core component, dot-product attention with softmax normalization, enables transformers to capture long-range dependencies effectively. However, this comes at the cost of quadratic complexity $\mathcal{O}(N^2)$ in relation to the sequence length N , resulting in considerable computational overhead particularly when processing long-sequence videos or high-resolution images. This limits their efficiency in resource-constrained environments, making practical deployment difficult in such scenarios.

To mitigate this challenge, various methods have been proposed to *accelerate* attention computation. Techniques such as localized or sparse attention reduce the number of tokens or key-value pairs by restricting attention to smaller windows or sparser patterns, thereby lowering the overall computational costs. While effective, these methods often sacrifice important contextual information, leading to unstable convergence behaviors and performance degradation. As a more principled

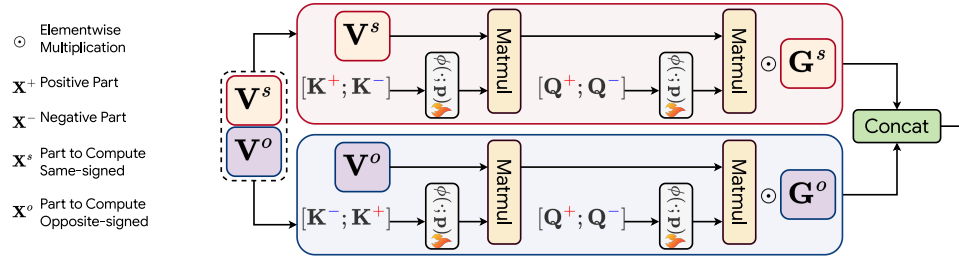


Figure 2: **The overall framework of PolaFormer.** Our framework explicitly separates query-key pairs based on their polarity into two distinct streams, with scaled outputs controlled by the learnable sign-aware matrices G^s and G^o for same-signed and opposite-signed components, respectively. A channel-wise power function with the learnable exponent p is employed to learn the rescaling process, capturing the sharpness characteristic of softmax.

solution, linear attention (Katharopoulos et al., 2020) replaces the Softmax operation in the query-key dot product with kernelized feature maps, effectively reducing time and space complexity from $\mathcal{O}(N^2d)$ to $\mathcal{O}(Nd^2)$, where d denotes the feature map dimension. Recent advances in linear attention have centered on designing two key components, *i.e.*, (1) *non-negative feature maps* such as ELU+1 (Katharopoulos et al., 2020) and ReLU (Qin et al., 2022) and (2) *kernel functions* including Gaussian kernels (Chen et al., 2021), Laplace kernels (Verma, 2021) and polynomial kernels (Kacham et al., 2024), to preserve the core properties of the original Softmax function while improving computational efficiency.

Despite the efficiency gains, linear attention still falls short in expressive capacity compared to softmax-based attention: As illustrated in Figure 1, it often yields more *uniform* attention weights across query-key pairs, thus resulting in reduced specificity. For instance, when querying a particular region like *bird wing*, linear attention tends to activate key tokens from unrelated areas (*e.g.*, *poles*) equally, introducing noise that disrupts downstream vision tasks. Our analysis identifies two primary causes for this shortfall, both stemming from **information loss** during the Softmax approximation:

(1) **Loss of Negative Values.** Linear attention models that rely on non-negative feature maps, such as ReLU, fail to maintain consistency with the original query-key dot product. These feature maps retain only *positive-positive* interactions, while crucial *negative-negative* and *positive-negative* interactions are completely dropped. This selective representation limits the model’s ability to capture a comprehensive range of relationships, leading to diminished expressiveness and reduced discriminative power in the resulting attention maps.

(2) **Loss of Attention Spikeness.** Without the exponential scaling of softmax, linear attention leads to more uniform weight distributions and lower entropy. This uniformity weakens the model’s ability to distinguish between strong and weak query-key pairs, impairing its focus on important features and reducing performance in tasks requiring fine detail.

In this work, we propose a polarity-aware linear attention (**PolaFormer**) mechanism, designed to address the limitations of prior linear attention models by incorporating the previously omitted negative interactions. Unlike traditional approaches that only preserve positive-positive query-key interactions, PolaFormer explicitly separates query-key pairs based on their polarity—handling a full spectrum of same-signed (*positive-positive*, *negative-negative*) and opposite-signed (*positive-negative*, *negative-positive*) interactions as shown in Figure 2. These interactions are processed in two streams, allowing for a more accurate reconstruction of the original softmax attention weights. To avoid unnecessary complexity, we split the value vector along the channel dimension, handling both types of interactions without introducing additional learnable parameters. The outputs are then concatenated and scaled with a learnable sign-aware matrix, ensuring a faithful reconstruction of query-key relationships.

To mitigate the issue of uniform attention weights commonly observed in linearized attention, we provide a theoretical foundation showing that an element-wise function can rescale the query-key responses to reduce entropy, provided the function has positive first and second derivatives. This insight helps clarify why previous feature maps such as ReLU and ELU tend to elevate entropy, leading to overly smoothed attention distributions. For simplicity, we employ a channel-wise learn-

able power function for rescaling, which retains the sharpness of the exponential function inherent in Softmax. This enables the model to capture spiky attention peaks, improving its ability to distinguish between strong and weak responses. Together, these enhancements offer a more robust solution to bridging the gap between linearized and softmax-based attention. We conduct extensive experiments on various vision tasks and the Long Range Arena benchmark (Tay et al., 2021), demonstrating that our model enhances performance by up to 4.6% while preserving a superior balance between expressive capability and efficiency.

2 RELATED WORK

Efficient Vision Transformers. By cutting images into smaller patches and processing them as a sequence, Vision Transformers (ViT) (Dosovitskiy et al., 2021) successfully transfer transformer models (Vaswani et al., 2017) from language tasks to vision tasks, and have achieved remarkable results. However, the quadratic complexity of the self-attention mechanism in ViT makes it expensive to train. Existing works have made various improvements to ViT for computational efficiency. Swin-Transformer (Liu et al., 2021) introduces a shifted windows scheme to limit self-attention computation to local windows. Pyramid Vision Transformer (PVT) (Wang et al., 2021) uses a progressive shrinking pyramid to reduce the computations of feature maps. DeiT (Touvron et al., 2021) enables models to achieve competitive performance without pretraining on large datasets by utilizing designed tokenization mechanisms and training strategies. However, these improvements do not solve the bottleneck of the self-attention mechanism, and quadratic complexity, thus the training cost is still unaffordable as the model scale increases. To address this issue, VMamba (Liu et al., 2024) extracts the information of the picture based on the spatial state model (SSM) encoding through serializing and scanning the picture, at the same time it inherits the linear complexity of SSM. VHeat (Wang et al., 2024) conceptualize image patches as heat sources and simulate the conduction process, and utilize DCT and IDCT operations to reduce the complexity to $\mathcal{O}(N^{1.5})$. These methods have just been proposed and are not yet as widely validated and deployed at scale as Transformers, [their model performance is also not significantly higher than the other models.](#)

KHpw.W2.2

Linear Attention. Sub-quadratic transformers focus on alleviating the inefficiency of the standard self-attention mechanism due to the softmax function and its quadratic complexity. A preferable solution is to use kernel-based similarities to reduce the complexity by approximating the softmax operator. The initial linear attention (Katharopoulos et al., 2020) proposes to substitute the Softmax function with a linear dot-product of kernel feature maps, which facilitates reducing the complexity from $\mathcal{O}(N^2)$ to $\mathcal{O}(N)$. Following this Softmax-free scheme, some variants of linear attention have been proposed by employing different kernel functions, such as ReLU(\cdot) (Shen et al., 2021) and $1 + \text{ELU}(\cdot)$ (Katharopoulos et al., 2020). Moreover, to fulfill the non-negative and distribution properties of attention matrix, Cosformer (Qin et al., 2022) combines the ReLU function and cos-based re-weighting mechanism to enhance the self-attention weights with locality inductive biases. FLatten Transformer (Han et al., 2023a) extends ReLU(\cdot) with power operation to maintain both properties of attention weights, *i.e.*, non-negative and low-entropy. It is a practical way to use power function to calculate the inner product to approximate exp, which is similar to the use of power function to [approximate max-pooling proposed in R-MAC \(Tolias et al., 2016\).](#) Recently, Agent Attention (Han et al., 2023b), a claimed generalized linear attention, introduces n agent tokens to aggregate features based on a combination of Softmax and linear attention with $\mathcal{O}(Nnd)$ complexity. As both N and n increase simultaneously with the model size, the complexity of the generalized linear attention is not absolutely linear with respect to N . Notably, the balanced performance still relies on the softmax operator and additional agent tokens, which violates the original premise of linear attention, *i.e.*, softmax-free and linear complexity. Current kernel functions either suffer from performance degradation or introduce excessive computational overhead. We observed significant information loss in comparison to original query-key dot products due to the non-negative constraint on attention weights and the intricate kernel designs aimed at achieving low entropy. This issue will be further addressed in the following sections of this work.

KHpw.W2.7

3 PRELIMINARY

In this section, we first highlight the inefficiency of the standard self-attention mechanism, followed by a discussion of the variants of existing linear attention methods.

3.1 LOW EFFICIENCY OF SELF-ATTENTION MECHANISM

Consider a sequence $\mathbf{x} \in \mathbb{R}^{N \times D}$ of token length N and dimension D . \mathbf{x} is divided into h heads, the dimension of each head is d . In each head, tokens at various positions are collectively attended to capture long-range dependencies. The output $\mathbf{O} = \{\mathbf{o}_t\}_{t=1}^N \in \mathbb{R}^{N \times d}$ can be formulated as:

$$\mathbf{O} = \text{Softmax}\left(\frac{\mathbf{Q}\mathbf{K}^\top}{\sqrt{d}}\right)\mathbf{V}, \quad \mathbf{o}_t = \frac{\sum_{i=1}^N \exp(\mathbf{q}_t \mathbf{k}_i^\top / \sqrt{d})}{\sum_{j=1}^N \exp(\mathbf{q}_t \mathbf{k}_j^\top / \sqrt{d})} \mathbf{v}_i. \quad (1)$$

Here, the query, key, and value vectors of dimension d are obtained by linearly projecting the inputs with three learnable matrices $\mathbf{Q} = \{\mathbf{q}_t\}_{t=1}^N$, $\mathbf{K} = \{\mathbf{k}_t\}_{t=1}^N$, $\mathbf{V} = \{\mathbf{v}_t\}_{t=1}^N \in \mathbb{R}^d$. For each head, the complexity of self-attention is $\mathcal{O}(N^2 d)$, making the mechanism inefficient for long sequences.

3.2 KERNEL-BASED LINEAR ATTENTION

To mitigate the efficiency bottlenecks of standard self-attention, kernel-based linear attention mechanisms (Katharopoulos et al., 2020) have been proposed, which decompose the similarity function into dot products of feature maps. Following the notations in (Choromanski et al., 2021; Chen et al., 2021), we define $\mathbf{SM}(\mathbf{q}, \mathbf{k}) = \exp(\mathbf{q}_i \mathbf{k}_j^\top)$ as the softmax kernel function. Mathematically, linear attention aims to use $\phi(\mathbf{q}_i) \phi(\mathbf{k}_j)^\top$ to approximate $\mathbf{SM}(\cdot, \cdot)$, where the feature map $\phi(\cdot) : \mathbb{R}^d \mapsto \mathbb{R}^{d'}$ is applied row-wise to the query and key matrices. As a result, the t -th row of attention output \mathbf{o}_t can be rewritten as,

$$\mathbf{o}_t = \frac{\sum_{i=1}^N \phi(\mathbf{q}_t) \phi(\mathbf{k}_i)^\top \mathbf{v}_i}{\sum_{j=1}^N \phi(\mathbf{q}_t) \phi(\mathbf{k}_j)^\top} = \frac{\phi(\mathbf{q}_t) \sum_{i=1}^N \phi(\mathbf{k}_i)^\top \mathbf{v}_i}{\phi(\mathbf{q}_t) \sum_{j=1}^N \phi(\mathbf{k}_j)^\top}. \quad (2)$$

By leveraging the associative property of matrix multiplication, the complexity per head is reduced to $\mathcal{O}(Nd'^2)$, which scales linearly with the sequence length.

Choices of Feature Map $\phi(\cdot)$. The primary distinction between various linear attention methods lies in the choice of feature maps $\phi(\cdot)$. Considering $\mathbf{SM}(\cdot, \cdot)$ is a PSD kernel function and the chosen feature map ϕ must satisfy two properties:

1. **Non-negativity.** To preserve the non-negative values in the approximation of \mathbf{SM} , previous methods utilize activation functions like $\phi(\mathbf{x}) = 1 + \text{ELU}(\mathbf{x})$ (Katharopoulos et al., 2020) or $\phi(\mathbf{x}) = \text{ReLU}(\mathbf{x})$ (Qin et al., 2022; Han et al., 2023a). Other approaches connect \mathbf{SM} with Gaussian kernel that uses $\phi(x) = \exp(\frac{\|\mathbf{x}\|^2}{2})$, incorporating trigonometric or random positive features.
2. **Low Entropy.** It has been observed the attention-weights distribution in standard Transformers tends to be more ‘‘spiky’’ in linear ones, exhibiting lower entropy (Zhang et al., 2024a). To rescale the query-key dot products back to the original magnitudes, techniques such as Taylor expansion (Keles et al., 2023) or higher norms on the numerical value of query and key (Han et al., 2023a) have been employed.

However, using non-negative feature maps inherently results in the loss of information from the original *negative* values, which may carry important information in the original dot product calculation. This leads to discontinuities in the linear attention map compared to the standard attention. Furthermore, existing rescaling strategies (Han et al., 2023a) manually select a fixed norm across all dimensions, i.e., $\phi(\mathbf{x}) = f_p(\text{ReLU}(\mathbf{x}))$, where $f_p(\mathbf{x}) = \frac{\|\mathbf{x}\|}{\|\mathbf{x}\|^p} \mathbf{x}^p$. This fixed norm p may not be optimal across different datasets.

4 PROPOSED APPROACH

In this section, we present a novel polarity-aware attention mechanism that accurately captures query-key interactions without incurring additional computational overhead. Our method incorporates a learnable dimension-wise power function that dynamically rescales the magnitudes of same- and opposite-signed components, effectively reducing entropy in the linear attention.

4.1 POLARITY-AWARE ATTENTION

The key idea behind polarity-aware attention is to address the limitations of existing linear attention mechanisms, which often discard valuable information from negative components. We start by decomposing the query vector $\mathbf{q} = \{q_i\}_{i \in [d]} \in \mathbb{R}^d$ and key vector $\mathbf{k} = \{k_i\}_{i \in [d]} \in \mathbb{R}^d$ element-wise into their positive and negative components:

$$\mathbf{q} = \mathbf{q}^+ - \mathbf{q}^-, \quad \mathbf{k} = \mathbf{k}^+ - \mathbf{k}^-, \quad (3)$$

where $\mathbf{q}_i^+ = \max(q_i, 0)$ and $\mathbf{q}_i^- = \max(-q_i, 0)$, representing the positive and negative parts of \mathbf{q} , respectively, and similarly for \mathbf{k} . Substituting these decompositions into the inner product of \mathbf{q} and \mathbf{k} gives:

$$\langle \mathbf{q}, \mathbf{k} \rangle = \underbrace{\langle \mathbf{q}^+, \mathbf{k}^+ \rangle + \langle \mathbf{q}^-, \mathbf{k}^- \rangle}_{\text{neglected negatives}} - \langle \mathbf{q}^+, \mathbf{k}^- \rangle - \langle \mathbf{q}^-, \mathbf{k}^+ \rangle \quad (4)$$

The first two terms capture the similarity between *same-signed* components, while the latter two terms represent interactions between *opposite-signed* components. Previous linear attention approaches, such as ReLU-based feature maps, eliminate negative components by mapping them to zero, resulting in significant information loss when approximating query-key dot products.

To address this, our polarity-aware attention mechanism separates query-key pairs based on their polarity, computing their interactions *independently*. The attention weights are calculated as follows:

$$\begin{aligned} \text{SM}(\mathbf{q}, \mathbf{k}^\top) &= \exp(\mathbf{q}\mathbf{k}^\top) \\ &\approx (\phi(\mathbf{q}^+)\phi(\mathbf{k}^+))^\top + \phi(\mathbf{q}^-)\phi(\mathbf{k}^-)^\top - (\phi(\mathbf{q}^+)\phi(\mathbf{k}^-)^\top + \phi(\mathbf{q}^-)\phi(\mathbf{k}^+)^\top). \end{aligned} \quad (5)$$

This formulation recovers the information embedded in both positive and negative components.

Learnable Polarity-aware Mixing. While this formulation captures key information carried by both same-signed and opposite-signed components, directly subtracting opposite-signed similarities can violate non-negativity constraints, leading to unstable training and suboptimal performance. To avoid the pitfalls of subtractive operation, we instead resort to a learnable mixing mechanism that weighs the contributions of same-signed and opposite-signed query-key similarities.

More concretely, we split each value vector $\mathbf{v} \in \mathbb{R}^{N \times d}$ along the d dimension into two halves to separately handle same- and opposite-signed response, *i.e.*, $\mathbf{v} = [\mathbf{v}^s; \mathbf{v}^o]$, where both \mathbf{v}^s and \mathbf{v}^o have a dimensionality of $d/2$. The output attention is then computed as:

$$\mathbf{o}_t = \left[\frac{\phi([\mathbf{q}_t^+; \mathbf{q}_t^-]) \sum_{i=1}^N \phi([\mathbf{k}_i^+; \mathbf{k}_i^-])^\top \mathbf{v}_i^s}{\phi([\mathbf{q}_t^+; \mathbf{q}_t^-]) \sum_{j=1}^N \phi([\mathbf{k}_j^+; \mathbf{k}_j^-])^\top} \odot \mathbf{G}^s; \frac{\phi([\mathbf{q}_t^+; \mathbf{q}_t^-]) \sum_{i=1}^N \phi([\mathbf{k}_i^-; \mathbf{k}_i^+])^\top \mathbf{v}_i^o}{\phi([\mathbf{q}_t^+; \mathbf{q}_t^-]) \sum_{j=1}^N \phi([\mathbf{k}_j^-; \mathbf{k}_j^+])^\top} \odot \mathbf{G}^o \right], \quad (6)$$

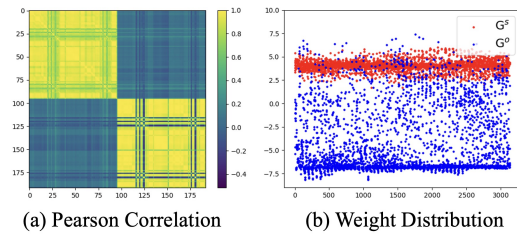


Figure 3: Visualizations of weights in \mathbf{G}^s and \mathbf{G}^o .

strategy compensates for the relaxed subtraction operation in Equation (5).

Low-Rank SM. Previous theoretical work (Verma, 2021) has shown that SM is inherently low-rank, particularly in higher layers where the spectrum distribution becomes more skewed. This property can lead to degenerate solutions when learning value vectors, especially when compact representations are required to accommodate polarity-aware information in our case. We explore various techniques such as depthwise and deformable convolutions to increase the rank, which can refer to the ablation study in Section 5.4.

4.2 REDUCING ENTROPY IN LINEAR ATTENTION VIA LEARNABLE POWER FUNCTIONS

Softmax-free linear attention mechanisms often exhibit higher entropy compared to softmax-based attention, leading to less sharp value vector attention, which is detrimental to tasks requiring precise

attention. To recover the low entropy characteristics observed in softmax-based attention, we reinterpret each row in $\text{SM}(\mathbf{q}, \mathbf{k}^\top)$ as a generalized unnormalized positive sequence $\mathbf{x} = (x_1, \dots, x_N)$ and analyze its entropy using our proposed positive sequence entropy (PSE) measure, defined as:

Definition 1 (Positive Sequence Entropy (PSE)). *Let a sequence $\mathbf{x} = (x_1, \dots, x_N)$, in which $x_i \geq 0$, $i = 1, \dots, N$, and $s = \sum_{i=1}^N x_i > 0$. Then the entropy of this positive sequence is defined by:*

$$\text{PSE}(\mathbf{x}) = - \sum_{i=1}^N \frac{x_i}{s} \log\left(\frac{x_i}{s}\right), \quad s = \sum_{i=1}^N x_i. \quad (7)$$

With $\text{PSE}(\cdot)$ defined, we now seek a function $g(\cdot)$ that can be applied element-wise to $\phi(\mathbf{q}^i)$ and $\phi(\mathbf{K}) = [\phi(\mathbf{k}^1), \dots, \phi(\mathbf{k}^N)]$ such that the PSE of the i -th row of the linear attention map is reduced. The following theorem formalizes the *conditions* under which this reduction in PSE can be achieved.

Theorem 1. *Let $\mathbf{x}, \mathbf{y}^n \in \mathbb{R}^d$ for $n = 1, \dots, N$, and let $g : [0, +\infty) \mapsto [0, +\infty)$ be a differentiable function satisfying the condition $g'(x) > 0$ and $g''(x) > 0$ for all $x > 0$. Then, there exists such a function g such that the PSE of the transformed sequence is strictly less than that of the original sequence. Specifically, we have:*

$$\text{PSE}(\langle g(\mathbf{x}), g(\mathbf{y}^1) \rangle, \dots, \langle g(\mathbf{x}), g(\mathbf{y}^N) \rangle) < \text{PSE}(\langle \mathbf{x}, \mathbf{y}^1 \rangle, \dots, \langle \mathbf{x}, \mathbf{y}^N \rangle). \quad (8)$$

Proof and supporting lemmas are provided in Section A.1.

This theorem also provides insights into why commonly used feature maps ϕ such as ReLU or ELU+1 fail to reduce entropy effectively, as they do not satisfy the necessary conditions of having both a positive first and second derivative across their entire domain.

To select a suitable function g , There exists a wide variety of functions g that meet these conditions. However, for the sake of model simplicity and efficiency, we opt for the most straightforward choice: a power function with an exponent greater than 1. Additionally, as different dimensions may contribute *unequally* to the similarity computation, we design learnable exponents to capture the varying importance of each dimension, formalized as follows:

$$\mathbf{p} = 1 + \alpha \text{sigmoid}(w_1, \dots, w_d), \quad g(\mathbf{x}; \mathbf{p}) = (x_1^{p_1}, \dots, x_d^{p_d}) \quad (9)$$

Complexity Analysis. We now analyze the complexity complexity of PolaFormer and demonstrate its linear complexity. Let d denote the number of channels, d' the dimensionality after kernelized, and k the kernel size of convolution ($d' = d$ since $g(\cdot)$ does just a element-wise mapping). The computational cost for query, key, value, coefficients \mathbf{G}^s and \mathbf{G}^o and outputs projections is $5Nd^2$. Performing matrix multiplication for $(\mathbf{Q}, \mathbf{K}, \mathbf{V})$ across each head requires $4Ndd'$. The convolution operation contributes k^2Nd , while the element-wise multiplication of polarity-aware coefficients \mathbf{G}^s and \mathbf{G}^o requires Nd computations. Summarizing these components, the total complexity of PolaFormer is given in Equation (10), confirming its linear complexity *w.r.t.* sequence length N .

$$\Omega = \underbrace{5Nd^2}_{\text{Proj}} + \underbrace{4Ndd'}_{\text{Pola Attn}} + \underbrace{k^2Nd}_{\text{Conv}} + \underbrace{Nd}_{\text{coeff}} \quad (10)$$

5 EXPERIMENTS

In this section, we evaluate our PolaFormer model on three tasks: image classification on ImageNet-1K (Deng et al., 2009), object detection and instance segmentation on COCO (Lin et al., 2014), and semantic segmentation on ADE20K (Zhou et al., 2019), comparing its performance with previous efficient vision models. Additionally, we assess PolaFormer on the Long Range Arena (LRA) task (Tay et al., 2021) to compare against other linear attention models. [We first train PolaFormer from scratch on the image classification task, then fine-tune the pre-trained model on ADE20K dataset for segmentation and COCO dataset for detection.](#) The models were pretrained on 8 NVIDIA A800 GPUs and fine-tuned on 8 NVIDIA RTX A6000 and 8 NVIDIA RTX 3090 GPUs.

5.1 IMAGENET-1K CLASSIFICATION

The ImageNet-1K (Deng et al., 2009) dataset is the widely used dataset for image classification tasks, containing 1,000 categories and over 1.2 million training images. We comprehensively assess our model’s performance using Top-1 accuracy, and compare it against recent state-of-the-art

Table 1: Comparison of various linear attention methods relative to the original models (DeiT-T and Swin-T) on the ImageNet-1K dataset, with the best results highlighted in boldface.

METHOD	RESO	PARAMS	FLOPs	ACC(%)
DeiT (Touvron et al., 2021)	224 ²	5.7M	1.1G	72.2
DeiT-EfficientAttn (Shen et al., 2021)	224 ²	5.7M	1.1G	70.2
DeiT-HydraAttn (Bolya et al., 2022)	224 ²	5.7M	1.1G	68.3
DeiT-EnhancedAttn (Cai et al., 2022)	224 ²	5.8M	1.1G	72.9
DeiT-AngularAttn (You et al., 2023)	224 ²	5.7M	1.1G	70.8
DeiT-FLattenAttn (Han et al., 2023a)	224 ²	6.1M	1.1G	74.1
DeiT-MobiAttn (Yao et al., 2024)	224 ²	5.7M	1.2G	73.3
DeiT-PolaFormer	224 ²	6.1M	1.2G	74.6 _{+2.4}
Swin (Liu et al., 2021)	224 ²	28M	4.4G	81.2
Swin-HydraAttn (Bolya et al., 2022)	224 ²	29M	4.5G	80.7
Swin-EfficientAttn (Shen et al., 2021)	224 ²	29M	4.5G	81.0
Swin-LinearAngularAttn (You et al., 2023)	224 ²	29M	4.5G	79.4
Swin-EnhancedAttn (Cai et al., 2022)	224 ²	29M	4.5G	81.8
Swin-FLattenAttn (Han et al., 2023a)	224 ²	29M	4.5G	82.1
Swin-PolaFormer	224 ²	29M	4.5G	82.6 _{+1.4}

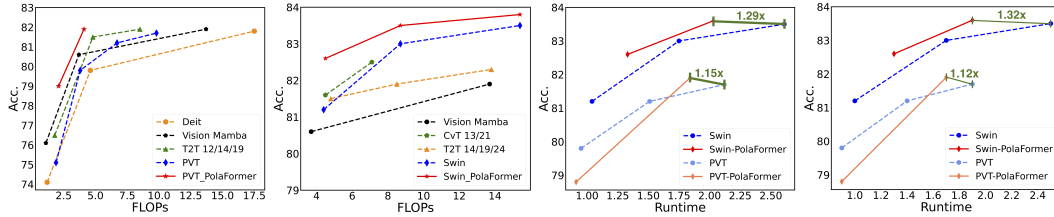


Figure 4: Efficiency analysis with Accuracy vs. FLOPs and Accuracy vs. Runtime curves on the ImageNet-1K dataset.

efficient Vision Transformer (ViT) models. Specifically, we selected four representative ViT backbones: DeiT (Touvron et al., 2021), PVT (Wang et al., 2021), PVTv2 (Wang et al., 2022) and Swin-Transformer (Liu et al., 2021). We replaced their self-attention modules with the our proposed polarity-aware attention module and trained these Pola-variants from scratch on ImageNet-1K.

Results. The experimental results are presented in Table 1 and Table 5, consistently showing that our model outperforms the baseline models. For instance, in Table 1, our DeiT-T-PolaFormer surpasses other DeiT variants from 0.5% to 6.3%. In Table 5, the PVT-T/S-PolaFormer obtain an increase of 3.7% and 2.1% comparing with the corresponding baseline with comparable FLOPs. Additionally, our method integrated in Swin and PVTv2 achieves a better balance between performance and efficiency. These results demonstrate that the PolaFormer enhances the expressive capability of the attention mechanism and can be widely applied in various attention-based models.

Efficiency Analysis. We visualize the efficiency comparison between the proposed PolaFormer and other linear attention approaches with similar FLOPs in the first two plots of Figure 4. The results show that our model can achieve comparable performance with significantly less computation. Furthermore, we evaluate the inference speed of PolaFormer. To be specific, we test the PVT-PolaFormer and Swin-PolaFormer on RTX3090 and RTX6000 platforms, as shown in the third and forth plots of Figure 4. PVT-PolaFormer achieves 1.15 \times and 1.12 \times faster inference speed and Swin-PolaFormer achieves 1.32 \times and 1.29 \times faster, both with comparable or higher accuracy. These figures highlight the excellent trade-off between accuracy and latency that our model provide.

5.2 OBJECT DETECTION AND INSTANCE SEGMENTATION

We further validate the effectiveness of the proposed approach across various vision tasks, including object detection task on the COCO dataset (Lin et al., 2014), which contains over 118K training images and 5K validation images. We integrate Pola-Swin and Pola-PVT separately as the backbone into Mask-RCNN (M) (He et al., 2017), RetinaNet (R) (Lin et al., 2017) and Cascade Mask R-CNN (C) Cai & Vasconcelos (2021) implementations and evaluate their performance based on the ImageNet-1k pretrained weights. As shown in Table 2 (left), our model consistently outperforms the original backbones under all settings, achieving notable improvements in all metrics. For instance,

Table 2: Object detection and instance segmentation results on the COCO dataset. The “Type” column specifies the detector used: R represents RetinaNet, M for Mask R-CNN, and C for Cascade Mask R-CNN. For semantic segmentation on the ADE20K dataset (last column), two encoder types are employed: S corresponds to Semantic FPN, and U refers to UperNet.

METHOD	DETECTION AND INSTANCE SEGMENTATION								SEMANTIC SEG	
	SCH.	TYPE	AP ^b	AP ^b ₅₀	AP ^b ₇₅	AP ^m	AP ^m ₅₀	AP ^m ₇₅	TYPE	mIoU(%)
PVT-T	1×	R	36.7	-	-	-	-	-	S	35.7
	1×	M	36.7	59.2	39.3	35.1	56.7	37.3		
PVT-T-Flatten	1×	R	-	-	-	-	-	-	S	37.2
	1×	M	38.2	61.6	41.9	37.0	57.6	39.0		
PVT-T-PolaFormer	1×	R	39.5 _{+2.8}	60.1	42.1	-	-	-	S	38.3 _{+2.6}
	1×	M	40.4 _{+3.7}	62.4 _{+3.2}	43.9 _{+4.6}	37.4 _{+2.3}	59.4 _{+2.7}	40.3 _{+3.0}		
PVT-S	1×	R	40.4	-	-	-	-	-	S	39.8
	1×	M	40.4	62.9	43.8	37.8	60.1	40.3		
PVT-S-PolaFormer	1×	R	43.2 _{+2.8}	64.1	46.4	-	-	-	S	41.0 _{+1.2}
	1×	M	43.9 _{+3.5}	66.1 _{+3.2}	47.9 _{+4.1}	40.2 _{+2.4}	63.1 _{+3.0}	43.0 _{+2.7}		
Swin-T	1×	M	43.7	66.6	47.7	39.8	63.3	42.7	U	44.5
	3×	M	46.0	68.1	50.3	41.6	65.1	44.9		
	3×	C	50.4	69.2	54.7	43.7	66.6	47.3		
Swin-T-FLatten	1×	M	44.2	67.3	48.5	40.2	63.8	43.0	U	44.8
	3×	M	46.5	68.5	50.8	42.1	65.4	45.1		
	3×	C	50.8	69.6	55.1	44.1	67.0	48.1		
Swin-T-PolaFormer	1×	M	44.8 _{+1.1}	67.6 _{+1.0}	49.1 _{+1.4}	40.5 _{+0.7}	64.1 _{+0.8}	43.5 _{+0.7}	U	45.8 _{+1.3}
	3×	M	47.0 _{+1.0}	68.9 _{+0.8}	51.5 _{+1.2}	42.3 _{+0.7}	66.0 _{+0.9}	45.8 _{+0.9}		
	3×	C	51.1 _{+0.7}	70.0 _{+0.8}	55.6 _{+0.9}	44.4 _{+0.7}	67.3 _{+0.7}	48.3 _{+1.0}		

our PVT-T-PolaFormer tested with both R and M detectors, surpasses the baselines from 2.3% to 4.6%. Additionally, our Swin-T-PolaFormer achieves 49.1% in AP^b₇₅, showing a 1.4% improvement compared to the original Swin-T with M detector. We additionally evaluate PVT-S-PolaFormer with R and M detectors, and Swin-T-PolaFormer with M and C detectors using 1× and 3× schedule. Compared to classification tasks, our model delivers more substantial performance gains on detection, which demands fine-grained attention maps for accurate localization of bounding boxes. Our model captures previously omitted interactions involving negative values and better restores attention maps with appropriate scales, effectively distinguishing between similar and dissimilar query-key relationships.

5.3 SEMANTIC SEGMENTATION

A similar phenomenon was observed when fine-tuning our pre-trained model for pixel-wise semantic segmentation tasks on the ADE20K dataset. ADE20K (Zhou et al., 2019) provides a diverse set of annotations for scenes, objects, and object parts, containing 25,000 images of complex scenes with various objects in natural spatial environments. We integrate Pola-Swin and Pola-PVT with ImageNet-1K pre-trained weights into two segmentation models, SemanticFPN (Kirillov et al., 2019) and UperNet (Xiao et al., 2018), using mIoU as the evaluation metric. The results, shown in Table 2 (right), demonstrate a performance improvement in mIoU ranging from 1.2% to 2.6%. These findings further highlight the versatility of our model, showing that it can be effectively fine-tuned and adapted to a wide range of vision tasks.

5.4 ABLATION STUDY

Table 3: Ablation study on each module using DeiT-T on ImageNet-1K.

POLARITY	G ^s , G ^o	DWC	DCN	ACC. (%)
✓	✓		✓	61.9 _{-12.7}
✓				68.1 _{-6.5}
✓		✓		72.8 _{-1.8}
✓	✓	✓		74.6

ity, achieving an accuracy of 74.6%. It is important to note that our model is agnostic to the choice of convolution modules. Furthermore, adopting polarity coefficients G^s and G^o yields a 1.8% improvement in row 3 and 4, indicating that the model effectively learns the complementary relationship between same-signed and opposite-signed values.

Comparison with Other Linear Attention. To compare with other linear attention models, we evaluate our PolaFormer on the Long Range Arena (LRA) (Tay et al., 2021) task, which is composed

Table 4: Comparisons (%) between the proposed PolaFormer and other linear attention models on LRA, with the best results are highlighted in boldface.

MODEL	TEXT	LISTOPS	RETRIEVAL	PATHFINDER	IMAGE	AVERAGE
Transformer	61.55	38.71	80.93	70.39	39.14	58.14
LocalAttn	52.98	15.82	53.39	66.63	41.46	46.06
LinearTrans.	65.90	16.13	53.09	75.30	42.34	50.55
Reformer	56.10	37.27	53.40	68.50	38.07	50.67
Performer	65.40	18.01	53.82	77.05	42.77	51.41
Synthesizer	61.68	36.99	54.67	69.45	41.61	52.88
Longformer	62.85	35.63	56.89	69.71	42.22	53.46
Informer	62.13	37.05	79.35	56.44	37.86	54.57
Bigbird	64.02	36.05	59.29	74.87	40.83	55.01
Linformer	57.29	36.44	77.85	65.39	38.43	55.08
Kernelized	60.02	38.46	82.11	69.86	32.63	56.62
Cosformer	63.54	37.2	80.28	70.00	35.84	57.37
Nystrom	62.36	37.95	80.89	69.34	38.94	57.90
Skyformer	64.70	38.69	82.06	70.73	40.77	59.39
Hedgehog	64.60	37.15	82.24	74.16	40.15	59.66
PolaFormer $_{\alpha=3}$	73.06	37.35	80.50	70.53	42.15	60.72
PolaFormer $_{\alpha=5}$	72.33	38.76	80.37	68.98	41.91	60.47
PolaFormer $_{\alpha=7}$	71.93	37.60	81.47	69.09	42.77	60.57

with five tasks: ListOps (Nangia & Bowman, 2018), Text Classification on IMDB review dataset (Maas et al., 2011), Document Retrieval on AAN dataset (Radev et al., 2013), Pathfinder (Linsley et al., 2018), and Image Classification on CIFAR-10 (Krizhevsky, 2009). The sequence length in both TEXT and RETRIEVAL tasks is 4k, in LISTOPS is 2k and in PATHFINDER and IMAGE is 1k. Following the setup of Skyformer (Chen et al., 2021), we adopt a comparable number of parameters and train the entire model end-to-end with the task-specific losses. Results for different scaling factors α of PolaFormer are shown in the bottom rows of Table 4. PolaFormer $_{\alpha=3}$ obtains the highest accuracy 73.06% in Text Classification task, PolaFormer $_{\alpha=5}$ has achieved the state-of-the-art results in ListOps task for 38.76% accuracy and the PolaFormer $_{\alpha=7}$ gains the best performance in Image Classification task with an accuracy of 42.77%. It is worth mentioning that PolaFormer $_{\alpha=3}$ achieves the highest overall scores on LRA benchmark, with all variants outperforming other linear attention models. Our model achieves better scores in linear complexity relying on its extraction ability and higher rank, showing great potential in both NLP and CV tasks.

Impact of Learnable Scaling. In Equation (9), we introduce the scaling factor α in our learnable power function, and analyze the effect of exponent \mathbf{p} on the model performance. The value of α primarily depends on the model size and context length. As the model size increases, a larger α is required to effectively select the most relevant tokens from long sequences, thereby reducing information entropy. We evaluate the model with $\alpha = 3, 5, 7$ on the LRA task, shown at the bottom of Table 4. Although PolaFormer $_{\alpha=3}$ achieves the best performance, in practice, for classification tasks, the results are relatively insensitive to variations in α , with a difference of no more than 2%.

6 CONCLUSION

In this work, we presented PolaFormer, a novel efficient transformer with linear complexity. Our PolaFormer is built on two properties of the original softmax attention: (i) making each element of the attention weight non-negative and (ii) making attention weight spikier. To fulfill these properties, we computed the similarity in a polarity-aware form to avoid neglecting negatives; theoretically, we proposed a family of element-wise functions to lower the entropy and employ a learnable power function for simplicity and rescaling. Besides, we used convolution to alleviate the problem of degenerate solutions caused by the low-rank property of SM and introduced polarity-aware coefficient matrices to learn the complementary relationship between same-signed and opposite-signed values. We validated the effectiveness of the proposed PolaFormer in a series of vision tasks and additionally benchmarked on the LRA testbed to fairly compare with mainstream linear attention models. The experimental results demonstrated that our model has good compatibility with most attention-based models and measures up to a better balance between performance and efficiency.

Table 5: Comparison of classification results on the ImageNet-1K dataset. The default input resolution is 224^2 , except for the last row, which reports results for variants using a resolution of 384^2 .

MODEL	RESO	PARAMS	FLOPs	ACC(%)
SBCFormer-B (Lu et al., 2024)	224^2	14M	1.6G	80.0
SBCFormer-L (Lu et al., 2024)	224^2	19M	2.7G	81.1
CAS-ViT-T (Zhang et al., 2024b)	224^2	22M	3.5G	82.3
VisionMamba-T (Zhu et al., 2024)	224^2	7M	1.1G	76.1
VisionMamba-S (Zhu et al., 2024)	224^2	26M	3.7G	80.6
VisionMamba-B (Zhu et al., 2024)	224^2	98M	13.7G	81.9
T2T-14 (Yuan et al., 2021a)	224^2	21.5M	4.8G	81.5
T2T-19 (Yuan et al., 2021a)	224^2	39.2M	8.5G	81.9
T2T-24 (Yuan et al., 2021a)	224^2	64.1M	13.8G	82.3
CvT-13(Wu et al., 2021)	224^2	20M	4.5G	81.6
CvT-21 (Wu et al., 2021)	224^2	32M	7.1G	82.5
CvT-13 (Wu et al., 2021)	384^2	20M	16.3G	83.0
CvT-21 (Wu et al., 2021)	384^2	32M	24.9G	83.3
HiViT-T (Zhang et al., 2023)	224^2	19M	4.6G	82.1
HiViT-S (Zhang et al., 2023)	224^2	38M	9.1G	83.5
HiViT-B (Zhang et al., 2023)	224^2	66M	15.9G	83.8
PVT-T-FLatten (Han et al., 2023a)	224^2	11M	1.9G	77.8
PVT-S-FLatten (Han et al., 2023a)	224^2	22M	4.0G	81.7
PVTv2-b0-FLatten (Han et al., 2023a)	224^2	3.2M	0.6G	71.1
PVTv2-b0-MobiAtt (Yao et al., 2024)	224^2	3.5M	0.6G	71.5
PVTv2-b1-FLatten (Han et al., 2023a)	224^2	13M	2.2G	79.5
Swin-S-FLatten (Han et al., 2023a)	224^2	51M	8.7G	83.5
Swin-B-FLatten (Han et al., 2023a)	224^2	89M	15.4G	83.8
PVT-T (Wang et al., 2021)	224^2	13M	1.9G	75.1
PVT-T-PolaFormer	224^2	12M	2.0G	78.8 _{+3.7}
PVT-S (Wang et al., 2021)	224^2	25M	3.8G	79.8
PVT-S-PolaFormer	224^2	21M	4.1G	81.9 _{+2.1}
PVTv2-b0 (Wang et al., 2022)	224^2	3.7M	0.5G	70.5
PVTv2-b0-PolaFormer	224^2	3.4M	0.6G	72.3 _{+1.8}
PVTv2-b1 (Wang et al., 2022)	224^2	13M	2.1G	78.7
PVTv2-b1-PolaFormer	224^2	13M	2.2G	80.2 _{+1.5}
Swin-S (Liu et al., 2021)	224^2	50M	8.7G	83.0
Swin-S-PolaFormer	224^2	50M	8.7G	83.6 _{+0.6}
Swin-B (Liu et al., 2021)	224^2	88M	15.4G	83.5
Swin-B-PolaFormer	224^2	88M	15.4G	83.8 _{+0.3}
Swin-S (Liu et al., 2021)	384^2	50M	25.2G	84.3
Swin-B (Liu et al., 2021)	384^2	88M	47.0G	84.5
Swin-S-PolaFormer	384^2	50M	25.5G	84.7 _{+0.4}

REFERENCES

- Daniel Bolya, Cheng-Yang Fu, Xiaoliang Dai, Peizhao Zhang, and Judy Hoffman. Hydra attention: Efficient attention with many heads. In *Computer Vision - ECCV 2022 Workshops - Tel Aviv, Israel, October 23-27, 2022, Proceedings, Part VII*, pp. 35–49. Springer, 2022.
- Han Cai, Chuang Gan, and Song Han. Efficientvit: Enhanced linear attention for high-resolution low-computation visual recognition. *arXiv preprint arXiv:2205.14756*, 2022.
- Zhaowei Cai and Nuno Vasconcelos. Cascade R-CNN: high quality object detection and instance segmentation. *IEEE Trans. Pattern Anal. Mach. Intell.*, 43(5):1483–1498, 2021.
- Yifan Chen, Qi Zeng, Heng Ji, and Yun Yang. Skyformer: Remodel self-attention with gaussian kernel and nystrom method. In Marc’Aurelio Ranzato, Alina Beygelzimer, Yann N. Dauphin, Percy Liang, and Jennifer Wortman Vaughan (eds.), *Advances in Neural Information Processing Systems (NeurIPS)*, pp. 2122–2135, 2021.
- Krzysztof Marcin Choromanski, Valerii Likhoshesterov, David Dohan, Xingyou Song, Andreea Gane, Tamás Szepesvári, Peter Hawkins, Jared Quincy Davis, Afroz Mohiuddin, Lukasz Kaiser, David Benjamin Belanger, Lucy J. Colwell, and Adrian Weller. Rethinking attention with performers. In *9th International Conference on Learning Representations (ICLR)*. OpenReview.net, 2021.
- MMCV Contributors. MMCV: OpenMMLab computer vision foundation. <https://github.com/open-mmlab/mmcv>, 2018.
- Jia Deng, Wei Dong, Richard Socher, Li-Jia Li, Kai Li, and Li Fei-Fei. Imagenet: A large-scale hierarchical image database. In *IEEE Computer Society Conference on Computer Vision and Pattern Recognition (CVPR)*, pp. 248–255, 2009.
- Alexey Dosovitskiy, Lucas Beyer, Alexander Kolesnikov, Dirk Weissenborn, Xiaohua Zhai, Thomas Unterthiner, Mostafa Dehghani, Matthias Minderer, Georg Heigold, Sylvain Gelly, Jakob Uszkoreit, and Neil Houlsby. An image is worth 16x16 words: Transformers for image recognition at scale. In *9th International Conference on Learning Representations (ICLR)*. OpenReview.net, 2021.
- Dongchen Han, Xuran Pan, Yizeng Han, Shiji Song, and Gao Huang. Flatten transformer: Vision transformer using focused linear attention. In *IEEE International Conference on Computer Vision (ICCV)*, pp. 5938–5948, 2023a.
- Dongchen Han, Tianzhu Ye, Yizeng Han, Zhuofan Xia, Shiji Song, and Gao Huang. Agent attention: On the integration of softmax and linear attention. *CoRR*, abs/2312.08874, 2023b.
- Kaiming He, Georgia Gkioxari, Piotr Dollár, and Ross B. Girshick. Mask R-CNN. In *IEEE International Conference on Computer Vision, ICCV 2017, Venice, Italy, October 22-29, 2017*, pp. 2980–2988. IEEE Computer Society, 2017.
- Praneeth Kacham, Vahab Mirrokni, and Peilin Zhong. Polysketchformer: Fast transformers via sketching polynomial kernels. In *Forty-first International Conference on Machine Learning (ICML)*, 2024.
- Angelos Katharopoulos, Apoorv Vyas, Nikolaos Pappas, and François Fleuret. Transformers are rnns: Fast autoregressive transformers with linear attention. In *Proceedings of the 37th International Conference on Machine Learning (ICML)*, volume 119, pp. 5156–5165, 2020.
- Feyza Duman Keles, Pruthvi Mahesakya Wijewardena, and Chinmay Hegde. On the computational complexity of self-attention. In *34th International Conference on Algorithmic Learning Theory*, volume 201, pp. 597–619, 2023.
- Alexander Kirillov, Ross Girshick, Kaiming He, and Piotr Dollár. Panoptic feature pyramid networks. In *Proceedings of the IEEE/CVF Conference on Computer Vision and Pattern Recognition (CVPR)*, pp. 6399–6408, 2019.

- A Krizhevsky. Learning multiple layers of features from tiny images. *Thesis, University of Tront*, 2009.
- Tsung-Yi Lin, Michael Maire, Serge J. Belongie, James Hays, Pietro Perona, Deva Ramanan, Piotr Dollár, and C. Lawrence Zitnick. Microsoft COCO: common objects in context. In *European Conference Computer Vision (ECCV)*, volume 8693, pp. 740–755, 2014.
- Tsung-Yi Lin, Priya Goyal, Ross B. Girshick, Kaiming He, and Piotr Dollár. Focal loss for dense object detection. In *IEEE International Conference on Computer Vision, ICCV 2017, Venice, Italy, October 22-29, 2017*, pp. 2999–3007. IEEE Computer Society, 2017.
- Drew Linsley, Junkyung Kim, Vijay Veerabadran, Charles Windolf, and Thomas Serre. Learning long-range spatial dependencies with horizontal gated recurrent units. In *Advances in Neural Information Processing Systems (NeurIPS)*, pp. 152–164, 2018.
- Yue Liu, Yunjie Tian, Yuzhong Zhao, Hongtian Yu, Lingxi Xie, Yaowei Wang, Qixiang Ye, and Yunfan Liu. Vmamba: Visual state space model. *CoRR*, abs/2401.10166, 2024.
- Ze Liu, Yutong Lin, Yue Cao, Han Hu, Yixuan Wei, Zheng Zhang, Stephen Lin, and Baining Guo. Swin transformer: Hierarchical vision transformer using shifted windows. In *IEEE International Conference on Computer Vision (ICCV)*, pp. 9992–10002, 2021.
- Ilya Loshchilov and Frank Hutter. Decoupled weight decay regularization. In *7th International Conference on Learning Representations (ICLR)*, 2019.
- Xiangyong Lu, Masanori Suganuma, and Takayuki Okatani. Sbcformer: Lightweight network capable of full-size imagenet classification at 1 FPS on single board computers. In *IEEE/CVF Winter Conference on Applications of Computer Vision (WACV)*, pp. 1112–1122. IEEE, 2024.
- Andrew L. Maas, Raymond E. Daly, Peter T. Pham, Dan Huang, Andrew Y. Ng, and Christopher Potts. Learning word vectors for sentiment analysis. In *The 49th Annual Meeting of the Association for Computational Linguistics: Human Language Technologies (ACL-HLT)*, pp. 142–150, 2011.
- Nikita Nangia and Samuel R. Bowman. Listops: A diagnostic dataset for latent tree learning. In *Proceedings of the 2018 Conference of the North American Chapter of the Association for Computational Linguistics (NAACL)*, pp. 92–99. Association for Computational Linguistics, 2018.
- Zhen Qin, Weixuan Sun, Hui Deng, Dongxu Li, Yunshen Wei, Baohong Lv, Junjie Yan, Lingpeng Kong, and Yiran Zhong. Cosformer: Rethinking softmax in attention. In *The Tenth International Conference on Learning Representations (ICLR)*. OpenReview.net, 2022.
- Dragomir R. Radev, Pradeep Muthukrishnan, Vahed Qazvinian, and Amjad Abu-Jbara. The ACL anthology network corpus. *Lang. Resour. Evaluation*, 47(4):919–944, 2013.
- Zhuoran Shen, Mingyuan Zhang, Haiyu Zhao, Shuai Yi, and Hongsheng Li. Efficient attention: Attention with linear complexities. In *IEEE Winter Conference on Applications of Computer Vision (WACV)*, pp. 3530–3538. IEEE, 2021.
- Yi Tay, Mostafa Dehghani, Samira Abnar, Yikang Shen, Dara Bahri, Philip Pham, Jinfeng Rao, Liu Yang, Sebastian Ruder, and Donald Metzler. Long range arena : A benchmark for efficient transformers. In *9th International Conference on Learning Representations (ICLR)*. OpenReview.net, 2021.
- Giorgos Tolias, Ronan Sifre, and Hervé Jégou. Particular object retrieval with integral max-pooling of CNN activations. In *4th International Conference on Learning Representations, ICLR 2016, San Juan, Puerto Rico, May 2-4, 2016, Conference Track Proceedings*, 2016.
- Hugo Touvron, Matthieu Cord, Matthijs Douze, Francisco Massa, Alexandre Sablayrolles, and Hervé Jégou. Training data-efficient image transformers & distillation through attention. In *Proceedings of the 38th International Conference on Machine Learning (ICML)*, volume 139, pp. 10347–10357, 2021.

- Ashish Vaswani, Noam Shazeer, Niki Parmar, Jakob Uszkoreit, Llion Jones, Aidan N. Gomez, Lukasz Kaiser, and Illia Polosukhin. Attention is all you need. In *Advances in Neural Information Processing Systems (NeurIPS)*, pp. 5998–6008, 2017.
- Madhusudan Verma. Revisiting linformer with a modified self-attention with linear complexity. *CoRR*, abs/2101.10277, 2021. URL <https://arxiv.org/abs/2101.10277>.
- Wenhai Wang, Enze Xie, Xiang Li, Deng-Ping Fan, Kaitao Song, Ding Liang, Tong Lu, Ping Luo, and Ling Shao. Pyramid vision transformer: A versatile backbone for dense prediction without convolutions. In *IEEE/CVF International Conference on Computer Vision (ICCV)*, pp. 548–558. IEEE, 2021.
- Wenhai Wang, Enze Xie, Xiang Li, Deng-Ping Fan, Kaitao Song, Ding Liang, Tong Lu, Ping Luo, and Ling Shao. PVT v2: Improved baselines with pyramid vision transformer. *Comput. Vis. Media*, 8(3):415–424, 2022.
- Zhaozhi Wang, Yue Liu, Yunfan Liu, Hongtian Yu, Yaowei Wang, Qixiang Ye, and Yunjie Tian. wheat: Building vision models upon heat conduction. *CoRR*, abs/2405.16555, 2024.
- Haiping Wu, Bin Xiao, Noel Codella, Mengchen Liu, Xiyang Dai, Lu Yuan, and Lei Zhang. Cvt: Introducing convolutions to vision transformers. In *2021 IEEE/CVF International Conference on Computer Vision, ICCV 2021, Montreal, QC, Canada, October 10-17, 2021*, pp. 22–31. IEEE, 2021.
- Tete Xiao, Yingcheng Liu, Bolei Zhou, Yuning Jiang, and Jian Sun. Unified perceptual parsing for scene understanding. In *Proceedings of the European Conference on Computer Vision (ECCV)*, pp. 418–434, 2018.
- Zhiyu Yao, Jian Wang, Haixu Wu, Jingdong Wang, and Mingsheng Long. Mobile attention: Mobile-friendly linear-attention for vision transformers. In *Forty-first International Conference on Machine Learning (ICML)*, 2024.
- Haoran You, Yunyang Xiong, Xiaoliang Dai, Bichen Wu, Peizhao Zhang, Haoqi Fan, Peter Vajda, and Yingyan Celine Lin. Castling-vit: Compressing self-attention via switching towards linear-angular attention at vision transformer inference. In *IEEE/CVF Conference on Computer Vision and Pattern Recognition, CVPR 2023, Vancouver, BC, Canada, June 17-24, 2023*, pp. 14431–14442. IEEE, 2023.
- Li Yuan, Yunpeng Chen, Tao Wang, Weihao Yu, Yujun Shi, Zihang Jiang, Francis E. H. Tay, Jiashi Feng, and Shuicheng Yan. Tokens-to-token vit: Training vision transformers from scratch on imagenet. In *2021 IEEE/CVF International Conference on Computer Vision, ICCV 2021, Montreal, QC, Canada, October 10-17, 2021*, pp. 538–547. IEEE, 2021a.
- Yuhui Yuan, Rao Fu, Lang Huang, Weihong Lin, Chao Zhang, Xilin Chen, and Jingdong Wang. Hrformer: High-resolution transformer for dense prediction. *CoRR*, abs/2110.09408, 2021b.
- Michael Zhang, Kush Bhatia, Hermann Kumbong, and Christopher Ré. The hedgehog & the porcupine: Expressive linear attentions with softmax mimicry. In *The Twelfth International Conference on Learning Representations, ICLR 2024, Vienna, Austria, May 7-11, 2024*. OpenReview.net, 2024a.
- Tianfang Zhang, Lei Li, Yang Zhou, Wentao Liu, Chen Qian, and Xiangyang Ji. Cas-vit: Convolutional additive self-attention vision transformers for efficient mobile applications. *CoRR*, abs/2408.03703, 2024b.
- Xiaosong Zhang, Yunjie Tian, Lingxi Xie, Wei Huang, Qi Dai, Qixiang Ye, and Qi Tian. Hivit: A simpler and more efficient design of hierarchical vision transformer. In *The Eleventh International Conference on Learning Representations, ICLR 2023, Kigali, Rwanda, May 1-5, 2023*. OpenReview.net, 2023.
- Bolei Zhou, Hang Zhao, Xavier Puig, Tete Xiao, Sanja Fidler, Adela Barriuso, and Antonio Torralba. Semantic understanding of scenes through the ADE20K dataset. *Int. J. Comput. Vis. (IJCV)*, 127(3):302–321, 2019.

Lianghui Zhu, Bencheng Liao, Qian Zhang, Xinlong Wang, Wenyu Liu, and Xinggang Wang. Vision mamba: Efficient visual representation learning with bidirectional state space model. In *Forty-first International Conference on Machine Learning (ICML)*, 2024.

A APPENDIX

This Appendix provides proof and supporting lemma for Theorem 1, followed by implementation details for various vision tasks. The source code is available in the supplementary material for reference.

- **Proof. A.1:** The mathematical proof and supporting lemmas of Theorem 1
- **Implementation Details. A.2:** Training settings for all experiments
- **Long Sequence Efficiency**
- **Comparison of the results of models with different G initializations**
- **Visualization of Attention Probability Distribution’s Entropy**
- **Visualization of Attention Maps**

A.1 PROOF OF THEOREM 1

Theorem. Let $\mathbf{x}, \mathbf{y}^n \in \mathbb{R}^d$ for $n = 1, \dots, N$, and dimensions are independently distributed. Given that $g : [0, +\infty) \mapsto [0, +\infty)$ is a differentiable function satisfying the condition $g'(x) > 0$ and $g''(x) > 0$ for all $x > 0$. Then, there exists such a function g such that the PSE of the transformed sequence is strictly less than that of the original sequence. Specifically, we have:

$$\text{PSE}(\langle g(\mathbf{x}), g(\mathbf{y}^1) \rangle, \dots, \langle g(\mathbf{x}), g(\mathbf{y}^N) \rangle) < \text{PSE}(\langle \mathbf{x}, \mathbf{y}^1 \rangle, \dots, \langle \mathbf{x}, \mathbf{y}^N \rangle). \quad (11)$$

Proof. We establish two lemmas to facilitate the proof of the main theorem.

Lemma 1. Let f be a function induced by $g : [0, +\infty) \mapsto [0, +\infty)$ with the conditions of $g'(x) > 0$ and $g''(x) > 0$, for all $x > 0$, defined as:

$$f(\langle \mathbf{x}, \mathbf{y} \rangle) := \langle g(\mathbf{x}), g(\mathbf{y}) \rangle \quad (12)$$

where $\mathbf{x}, \mathbf{y} \in \mathbb{R}^{d+}$, $g(\mathbf{x}) = (g(x_1), \dots, g(x_d))$. Then $f(x) > 0$, $f'(x) > 0$ and $f''(x) > 0$, for all $x \geq 0$.

Proof. Consider the element-wise function g for pairs of (\mathbf{x}, \mathbf{y}) with dimension d :

$$\begin{aligned} g(\mathbf{x}) &= (g(x_1), \dots, g(x_d)) \\ g(\mathbf{y}) &= (g(y_1), \dots, g(y_d)) \end{aligned} \quad (13)$$

Then, the inner-product between $g(\mathbf{x})$ and $g(\mathbf{y})$ is given by,

$$\langle g(\mathbf{x}), g(\mathbf{y}) \rangle = \sum_{i=1}^d g(x_i)g(y_i). \quad (14)$$

Because of the independence across dimensions, we apply Jensen’s inequality, leveraging $g'(x) > 0$ and $g''(x) > 0$, yielding:

$$\begin{aligned} \mathbb{E}[f(\langle \mathbf{q}, \mathbf{k} \rangle)] &= \mathbb{E}[\langle g(\mathbf{q}), g(\mathbf{k}) \rangle] = \mathbb{E}\left[\sum_{i=1}^d g(q_i)g(k_i)\right] \\ &= \sum_{i=1}^d \mathbb{E}[g(q_i)g(k_i)] = \sum_{i=1}^d \mathbb{E}[g(q_i)]\mathbb{E}[g(k_i)] \\ &\leq \sum_{i=1}^d g(\mathbb{E}[q_i])g(\mathbb{E}[k_i]) \quad (\text{Jensen's Inequality}) \\ &= \langle g(\mathbb{E}[\mathbf{q}]), g(\mathbb{E}[\mathbf{k}]) \rangle = f(\langle \mathbb{E}[\mathbf{q}], \mathbb{E}[\mathbf{k}] \rangle) \\ &= f(\mathbb{E}[\langle \mathbf{q}, \mathbf{k} \rangle]) \end{aligned} \quad (15)$$

where $\mathbb{E}[\mathbf{q}] = (\mathbb{E}[q_1], \dots, \mathbb{E}[q_d])$ denotes a vector. Consequently, we have the following results, *i.e.*,

$$\mathbb{E}[f(\langle \mathbf{q}, \mathbf{k} \rangle)] \leq f(\mathbb{E}[\langle \mathbf{q}, \mathbf{k} \rangle]), \quad (16)$$

indicating that f is concave function having a positive second derivative. Also, according to the definition of \mathbf{x} and \mathbf{y} , f is obviously mapping from $[0, +\infty)$ to $[0, +\infty)$ with a positive first derivative.

□

Lemma 2. *Given two positive values (a, b) , and function $f : [0, +\infty) \mapsto [0, +\infty)$ with the conditions of $f'(x) > 0$ and $f''(x) > 0$, we have $\text{PSE}(f(a), f(b)) \leq \text{PSE}(a, b)$.*

Proof. Consider the case $N = 2$ (extendable to $N > 2$). Without loss of generality, we assume $a > b$, $c := \frac{a}{b}$, then $c > 1$, and $\text{PSE}(a, b)$ can be calculated as

$$\begin{aligned} H_1 &= -\left(\frac{a}{a+b} \log\left(\frac{a}{a+b}\right) + \frac{b}{a+b} \log\left(\frac{b}{a+b}\right)\right) \\ &= -\left(\frac{c}{c+1} \log\left(\frac{c}{c+1}\right) + \frac{1}{c+1} \log\left(\frac{1}{c+1}\right)\right) \\ &= \log(c+1) - \frac{c}{c+1} \log(c) \end{aligned} \quad (17)$$

Then, we apply the kernel function f on (a, b) , and it is mapped to $(f(a), f(b))$. Then, we define d by $d := \frac{f(a)}{f(b)}$, and it is easy to prove that $d > c > 1$. Followed by Eq. (17), we can compute $\text{PSE}(f(a), f(b))$ as:

$$H_2 = \log(d+1) - \frac{d}{d+1} \log(d) \quad (18)$$

Through defining $h(x) = \log(x+1) - \frac{x}{x+1} \log(x)$, $x > 1$, we have

$$\begin{aligned} h'(x) &= -\frac{\log(x)}{(x+1)^2} \\ h'(x) &\leq 0, \quad x > 1 \end{aligned} \quad (19)$$

indicating that $H_1 = h(c) > H_2 = h(d)$ for all $x > 1$, *i.e.*, $H_2 < H_1$. Therefore, all functions that satisfy the conditions have the effect of entropy decrease. □

Now come back to the theorem. Firstly, we define f induced by g that

$$f(\langle \mathbf{x}, \mathbf{y} \rangle) = \langle g(\mathbf{x}), g(\mathbf{y}) \rangle \quad (20)$$

From Lemma 1, we know that f is a function with positive first and second derivative. Then by using Lemma 2, we have,

$$\text{PSE}(f(\langle \mathbf{x}, \mathbf{y}^1 \rangle), f(\langle \mathbf{x}, \mathbf{y}^2 \rangle)) < \text{PSE}(\langle \mathbf{x}, \mathbf{y}^1 \rangle, \langle \mathbf{x}, \mathbf{y}^2 \rangle) \quad (21)$$

Therefore, the scaling effect can be achieved by the element-wise computation based on a function g with positive first and second derivative. This allows for the removal of the softmax function, enabling linear complexity and lower entropy in the attention mechanism. □

A.2 IMPLEMENTATION DETAILS

Classification. In this task, we use the AdamW optimizer (Loshchilov & Hutter, 2019) to train all of our models for 400 epochs, including 20 epochs for linear warm-up. The basic learning rate is set to $1e-3$ for 1024 batch size. Additionally, we use a weight decay of $5e-2$. The training framework is developed on the top of the official Swin Transformer implementation made by Microsoft.

Object Detection. In this task, we utilize pretrained PVT models and Swin models on as the backbone and connect them to various detectors. Specifically, for the PVT model, we select from RetinaNet and Mask R-CNN as detectors, with the schedule set to $1\times$. For the Swin model, we

choose the detector from Mask R-CNN and Cascade Mask R-CNN as detectors, where models using Mask R-CNN are experimented with under both $1\times$ and $3\times$ schedule settings, while models using Cascade Mask R-CNN case are trained under the $3\times$ schedule. All experiments follow the `mmcv-detection` (Contributors, 2018) project. The training epoch is set to 12 per schedule and we use the AdamW optimizer with a learning rate of $1e-4$ and a weight decay of $1e-4$.

Semantic Segmentation. we employ pretrained PVT models and Swin models on two representative segmentation models, SemanticFPN and UperNet. The task is conducted based `mmcv-segmentation` (Contributors, 2018) project. The training iteration is set to 40000 for PVT-SFPN models, 160000 for Swin-UperNet models by using AdamW optimizer with a learning rate of $2e-4$ and a weight decay of $1e-3$.

Long Range Arena. We evaluate the PolaFormer based on the official implementation of Skyformer (Chen et al., 2021). For Listops and Text Classification, we set batch size to 32 with $1e-4$ learning rate. For Pathfinder, we set batch size to 128 with $5e-4$ learning rate. For Image Classification, we set batch size to 256 with $1e-4$ learning rate. For Retrieval sub-task, we set batch size to 16 with $2e-4$ learning rate. All models are trained from scratch using the AdamW optimizer.

A.3 LONG SEQUENCE EFFICIENCY

To evaluate the scalability of our model in such settings, we performed experiments on the Long-Range Arena (LRA) benchmark. These results demonstrate PolaFormer’s efficiency and scalability for both high-resolution vision tasks and long-sequence NLP applications.

KHpw
Wlefficiency
EBEw

Table 6: Throughput and Peak Memory of various models. A denotes the accuracy, T denotes the throughput of each model and M denotes the peak memory cost.

		Softmax	Kernelized	Nystrom	Linformer	Informer	Skyformer	Pola(ours)
Img (1k)	A	39.14	32.63	38.94	38.43	37.86	40.77	42.15
	T	736.36	862.32	1251.28	1613.19	85.85	923.04	1340.89
	M	9645	13013	5941	3471	5357	8091	4505
Path (1k)	A	70.39	69.86	69.34	65.39	56.44	70.73	70.53
	T	691.67	811.59	1125.08	1057.03	299.94	748.98	1065.63
	M	4831	6515	2980	1745	2687	4055	2286
List (2k)	A	38.71	38.46	37.95	36.44	37.05	38.69	37.35
	T	402.06	496.48	834.85	528.52	305.53	627.14	949.80
	M	4473	6084	1186	881	2737	1712	1151
Text (4k)	A	61.55	60.02	62.36	57.29	62.13	64.7	73.06
	T	252.06	327.27	1330.68	970.90	521.16	949.80	876.74
	M	17122	11720	2043	1742	5736	3082	1155
Retri (4k)	A	80.93	82.11	80.89	77.85	79.35	82.06	80.5
	T	116.30	144.83	496.48	424.18	142.94	348.60	344.93
	M	8947	10699	2011	1649	3399	2987	1139
Avg	A	58.14	56.62 -1.52	57.90 -0.24	55.08 -3.06	54.57 -3.57	59.39 $+1.25$	60.72 $+2.58$
	T	439.69	528.50 $\times 1.20$	1007.68 $\times 2.29$	918.77 $\times 2.09$	271.08 $\times 0.62$	719.51 $\times 1.80$	915.60 $\times 2.08$
	M	9003.6	9606.2 $\times 1.07$	2832.2 $\times 0.31$	1897.6 $\times 0.21$	3983.2 $\times 0.44$	3985.4 $\times 0.44$	2047.2 $\times 0.22$

A.4 COMPARISON OF THE RESULTS OF MODELS WITH DIFFERENT G INITIALIZATIONS

To assess the impact of G initialization on downstream tasks, we conducted additional experiments using five distinct initialization methods. These experiments were performed on a text classification (TEXT) task in Long Range Arena (LRA) with a sequence length of 4k, maintaining the same experimental setup as described in Table 4. The initialization strategies tested included Kaiming uniform, zero initialization, normal distribution ($\mathcal{N}(0, 1)$), uniform distribution ($\mathcal{U}(0, 1)$), and constant ones. The results are summarized in the table below:

veYX
Q2

Init Comparison	Kaiming Uniform	Zeros	Normal(0,1)	Uniform(0,1)	Ones
Acc	73.06	72.17	74.30	74.40	70.70

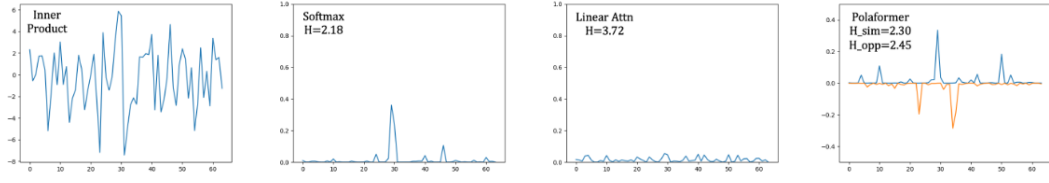


Figure 5: Visualization of different attention probability distributions

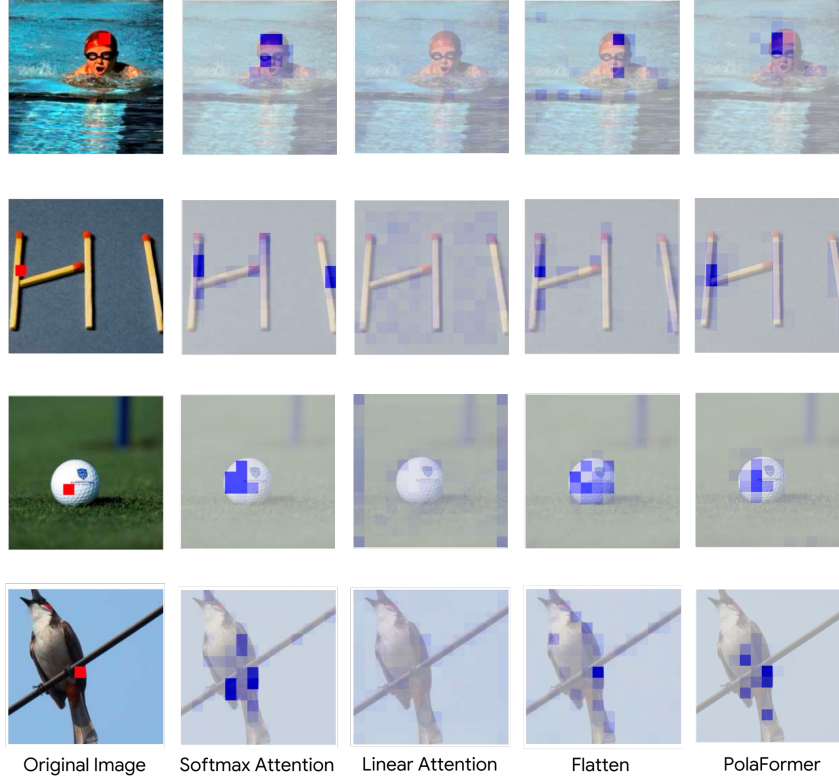


Figure 6: Visualization of the attention maps.

A.5 VISUALIZATION OF ATTENTION PROBABILITY DISTRIBUTION’S ENTROPY

We compute the entropy of standard self-attention, linear attention(Katharopoulos et al., 2020) and PolaFormer. Additionally, we visualize the distribution of one row of the Attention Score matrix, as shown in Fig5. It is clear that our model has a lower entropy than linear attention.

veYX
Q4

A.6 VISUALIZATION OF ATTENTION MAPS

To further show the characteristics of accurate similarity calculation and low information entropy of our model. We visualize more examples shown in Fig6. Thanks to the superiority of our designed kernel function, PolaFormer can calculate the similarity more accurately and focus on more relevant places.

veYX
Q5